NANO LETTERS

Letter

pubs.acs.org/NanoLett

Nonlinear Terahertz Absorption of Graphene Plasmons

Mohammad M. Jadidi,[*,†] Jacob C. König-Otto,[‡,¶] Stephan Winnerl,[‡] Andrei B. Sushkov,[§] H. Dennis Drew,[§] Thomas E. Murphy,[†] and Martin Mittendorff[†]

[†]Institute for Research in Electronics and Applied Physics, University of Maryland, College Park, Maryland 20742, United States

[‡]Helmholtz-Zentrum Dresden-Rossendorf, P.O. Box 510119, 01314 Dresden, Germany

[¶]Technische Universität Dresden, 01062 Dresden, Germany

[§]Center for Nanophysics and Advanced Materials, University of Maryland, College Park, Maryland 20742, United States

Supporting Information

ABSTRACT: Subwavelength graphene structures support localized plasmonic resonances in the terahertz and mid-infrared spectral regimes. The strong field confinement at the resonant frequency is predicted to significantly enhance the light-graphene interaction, which could enable nonlinear optics at low intensity in atomically thin, subwavelength devices. To date, the nonlinear response of graphene plasmons and their energy loss dynamics have not been experimentally studied. We measure and theoretically model the terahertz nonlinear response and energy relaxation dynamics of plasmons in graphene nanoribbons. We employ a terahertz pump–terahertz probe technique at the plasmon frequency and observe a strong saturation of plasmon absorption followed by a 10 ps relaxation time. The observed nonlinearity is enhanced by 2 orders of magnitude compared to unpatterned graphene with no plasmon resonance. We further present a thermal model for the nonlinear plasmonic absorption that supports the experimental results. The model shows that the observed strong linearity is caused by an unexpected red shift of plasmon resonance together with a broadening and weakening of the resonance caused by the transient increase in electron temperature. The model further predicts that even greater resonant enhancement of the nonlinear response can be expected in high-mobility graphene, suggesting that nonlinear graphene plasmonic devices could be promising candidates for nonlinear optical processing.

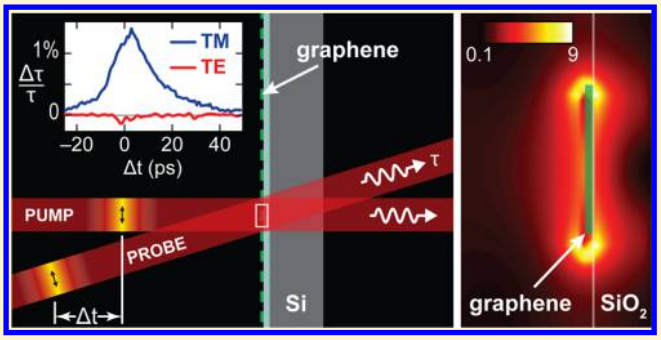

KEYWORDS: *Graphene, plasmons, nonlinear, pump–probe, terahertz*

Graphene exhibits a broadband intrinsic nonlinear optical response[1,2] that has been used in mode-locking[3] and harmonic generation.[4] In the optical and near-infrared regime, the nonlinear response of graphene is primarily attributed to transient Pauli blocking, which leads to an ultrafast saturable absorption and nonlinear refraction.[5] In the terahertz regime,[6,7] however, the nonlinear response is primarily caused by fast thermal heating and cooling of the electron population, which effects the intraband absorption.[8−10]

In the terahertz and mid-IR regime, the light-graphene interaction can be greatly increased by exploiting plasmon resonances, where the field is strongly localized and resonantly enhanced in a subwavelength graphene region.[11,12] A dramatic enhancement of the linear absorption has been experimentally observed in isolated subwavelength graphene elements[13−15] and graphene-filled metallic apertures[16] at resonant frequencies that can be controlled through the graphene dimensions and carrier concentration. Significant enhancement in the nonlinear response of graphene can be expected and has been theoretically predicted.[11,17−20] To date, there have been no experimental demonstrations to study this effect, or to explore the energy loss dynamics of these collective plasmonic excitations.

In this Letter, we measure the nonlinear response of plasmon resonances in an array of graphene nanoribbons using terahertz pump–terahertz probe measurements with a free-electron laser that is tuned to the plasmon resonance (9.4 THz.) We observe a resonantly enhanced pump-induced nonlinearity in the transmission that is orders of magnitude stronger than that of unpatterned graphene. The pump–probe measurements reveal an energy relaxation time of approximately 10 ps (measured at 20 K). We present a thermal model of the nonlinear plasmonic response that includes scattering through longitudinal acoustic (LA) phonons and disorder-assisted supercooling, which matches both the observed time scale and power-scaling of the nonlinear response.

The plasmonic devices were fabricated using chemical vapor deposition (CVD)-grown monolayer graphene that was

Received: January 29, 2016
Revised: March 7, 2016
Published: March 15, 2016

ACS Publications © 2016 American Chemical Society

DOI: 10.1021/acs.nanolett.6b00405
Nano Lett. 2016, 16, 2734−2738

transferred onto a 300 nm silicon oxide on lightly doped silicon (250 Ω·cm). Graphene ribbons with width w = 730 nm and period Λ = 1.5 μm were patterned using electron-beam lithography with a PMMA resist and oxygen plasma etch to remove the graphene from the exposed areas. The graphene grating covered a region of 1.5 × 1.5 mm. Figure 1a,b shows the

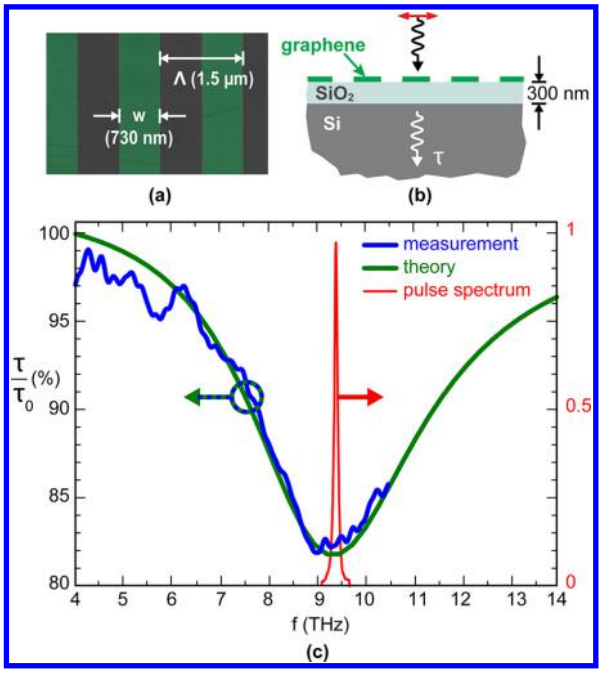

Figure 1. (a) False color scanning electron micrograph of fabricated graphene ribbons. (b) Cross sectional diagram of device. (c) Measured (blue) and best fit (green) linear transmission spectrum of device, showing a decreased transmission at the plasmon frequency of 9.4 THz. The superposed red curve shows the measured spectrum of the free-electron laser pulse source that was used to observe the nonlinear response.

structure, dimensions, and scanning-electron micrograph of the graphene plasmonic resonant structure considered here, and Figure 1c shows the measured room-temperature linear transmission spectrum of the sample, which exhibits a strong dip in transmission centered at 9.4 THz that is associated with plasmonic absorption of the nanoribbons.

The plasmon resonance can be approximated by assuming an equivalent sheet conductivity of the graphene ribbon array[21,22] (Supporting Information eq S9)

$$\sigma(\omega) = \frac{w}{\Lambda}\frac{D}{\pi\left[\Gamma - \frac{i(\omega^2 - \omega_p^2)}{\omega}\right]} \quad (1)$$

where Γ is the scattering rate and $D \simeq \sqrt{\pi n}\, e^2 v_F/\hbar$ is the Drude weight of graphene with a carrier concentration of n and Fermi velocity v_F. The plasmon resonant frequency is related to the Drude weight by $\omega_p^2 \equiv Dw/[2\Lambda^2\epsilon_0\bar{\epsilon}\ \ln(\sec(\pi w/2\Lambda))]$, where $\bar{\epsilon} = (\epsilon_1 + \epsilon_2)/2$ is the average of the substrate and incident dielectric constants.[21]

The relative power transmission through such a conductive sheet, accounting for reflection and transmission by the silicon substrate, is given by $\tau(\omega)/\tau_0 = |1 + \sigma(\omega)/(Y_1 + Y_2)|^{-2}$, where τ_0 denotes the transmission with the graphene film absent, and $Y_j \equiv (\epsilon_0\epsilon_j/\mu_0)^{1/2}$ is the admittance of the incident (j = 1) or substrate (j = 2) region (see Supporting Information eq S4.)

The green curve in Figure 1b shows the best-fit transmission spectrum calculated using this model, from which we determined the carrier concentration and graphene scattering rate to be $n = 9 \times 10^{12}$ cm^{-2} and Γ = 23 rad/ps, respectively, at room temperature, which corresponds to a Fermi energy of 0.35 eV and carrier mobility of 1250 cm^2 V^{-1} s^{-1}.

Figure 2 illustrates the experimental setup that was used to investigate the nonlinear terahertz response of the graphene

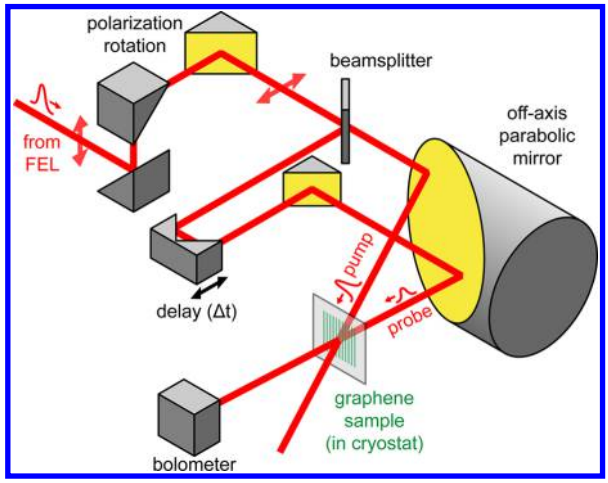

Figure 2. Sketch of the experimental setup for the pump−probe measurements. An optional reflective polarization rotation system orients the polarization perpendicular to the graphene ribbons. The pulses were separated into parallel, copolarized pump and probe pulses that were focused onto the graphene sample inside of a cryostat. The transmitted probe power was measured as a function of the relative pump−probe delay Δt, which was controlled through a mechanical delay stage.

plasmons. The free-electron laser (FEL) was tuned to produce 5.5 ps pulses with a repetition rate of 13 MHz that are resonant to the plasmon frequency of 9.4 THz. Compared to the plasmon resonance, the FEL radiation was spectrally narrow (cf. Figure 1c) The beam was split into pump and probe beams that were delayed relative to one another using a mechanical delay line. In all measurements, the pump and probe beams were copolarized, but the state of polarization could be set to be either perpendicular or parallel to the graphene ribbons in order to control whether or not the plasmons were excited, respectively. An off-axis parabolic mirror was employed to focus and overlap both beams at the graphene ribbon array. The sample was cooled to a (lattice) temperature of 20 K for all of the pump−probe measurements. While the emerging pump beam was extinguished, the intensity of the transmitted probe beam was measured using a cryogenically cooled bolometer as a function of the pump−probe delay Δt.

This signal, recorded as a function of the pump−probe delay Δt, is depicted in Figure 3a for several pump fluences. In all cases, the pump causes a transient increase in transmission that is accompanied by a decrease in absorption. The observed nonlinear response decays in the wake of the pump pulse with a time constant of ∼10 ps, which is close to the previously reported hot electron−phonon relaxation time in graphene at the measurement temperature (20 K).[23]

The electron temperature T in the graphene evolves in response to the terahertz pump pulse with intensity $I(t)$ at the center frequency ω_0 according to[24]

DOI: 10.1021/acs.nanolett.6b00405
Nano Lett. 2016, 16, 2734−2738

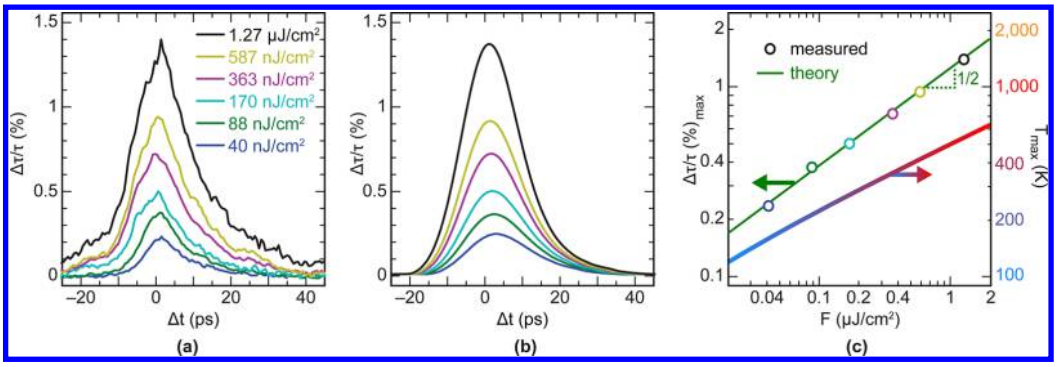

Figure 3. (a) Measured relative change in transmission of the probe signal for different pump fluences as a function of pump−probe time delay Δt. The positive signal indicates a decrease in absorption that becomes stronger at higher pump fluences. (b) Calculated relative change in transmission based on a nonlinear thermal model for plasmonic absorption in graphene nanoribbons that includes supercollision cooling and LA phonon scattering. (c) Measured and simulated peak of relative transmission change (left) and peak electron temperature (right) as a function of pump fluence F.

$$\alpha T\frac{\mathrm{d}T}{\mathrm{d}t} + \beta(T^3 - T_\mathrm{L}^3) = A(\omega_0;\, T)I(t) \tag{2}$$

where αT is the specific heat of graphene with $\alpha = 2\pi k_\mathrm{B}^2\varepsilon_\mathrm{F}/(3\hbar^2 v_\mathrm{F}^2)$, $\beta = \zeta(3)V_\mathrm{D}^2\varepsilon_\mathrm{F}k_\mathrm{B}^3/(\pi^2\rho\hbar^4 v_\mathrm{F}^3 s^2 l)$ is the cooling coefficient, T_L is the lattice temperature, $A(\omega_0;T)$ is the fractional absorption in the graphene, which itself depends on temperature. k_B is the Boltzmann constant, ρ is the areal mass density, s is the speed of sound in graphene, ζ is the Riemann zeta function, l is the electron-disorder mean free path, and V_D is the acoustic deformation potential. We assume that the temperature relaxation is dominated by disorder-assisted supercollision cooling $\propto T^3$,[24,25] rather than momentum-conserving cooling.[26]

The fractional absorption appearing in eq 2 can be derived from the equivalent conductivity eq 1 (Supporting Information eq S3),

$$A(\omega_0;\, T) = \frac{4Y_1\mathrm{Re}\{\sigma(\omega_0)\}}{|Y_1 + Y_2 + \sigma(\omega_0)|^2} \tag{3}$$

where ω_0 denotes the carrier frequency of the quasi-CW pump and probe pulses. The basis of the thermal model is that the Drude weight D, scattering rate Γ, and plasmon frequency appearing in eq 1 implicitly depend upon the electron temperature T, which increases when the incident pump pulse is absorbed in the graphene layer.

The temperature-dependent Drude weight[27,28] and plasmon frequency (Section S3) are calculated as

$$D(T) = \frac{2e^2}{\hbar^2}k_\mathrm{B}T\,\ln\left[2\cosh\left(\frac{\mu(T)}{k_\mathrm{B}T}\right)\right] \tag{4}$$

$$\omega_\mathrm{p}^2(T) = \frac{D(T)w}{2\epsilon_0\bar{\epsilon}\Lambda^2\ln\left(\sec\left(\frac{\pi w}{2\Lambda}\right)\right)} \tag{5}$$

The scattering rate Γ also varies with temperature, both because of temperature-dependent scattering from long-range Coulomb impurities and LA phonons[29]

$$\Gamma(T) = \frac{\Gamma_0\varepsilon_\mathrm{F}}{\mu(T)} + \frac{k_\mathrm{B}T\varepsilon_\mathrm{F}V_\mathrm{D}^2}{4\hbar^3 v_\mathrm{F}^2\rho s^2} \tag{6}$$

The second term in eq 6 describes the temperature dependent LA phonon scattering, which was essential in order to match the observed fluence dependence of the nonlinear response, shown in Figure 3c (see Section S4).

As the fast electron−electron scattering leads to a thermalization of the carrier distribution on a time scale of femtoseconds, we assume that the electron population maintains a Fermi distribution with a temperature that evolves in response to the terahertz pump pulse according to eq 2. The total electron population n must remain constant as the electrons heat and cool, which defines the following implicit relationship between the electron temperature and the chemical potential $\mu(T)$

$$n = \int_{-\infty}^{\infty}\frac{\nu(E)\mathrm{d}E}{1 + \exp\left[\frac{E-\mu(T)}{k_\mathrm{B}T}\right]} \tag{7}$$

where $\nu(E)$ is the density of states in graphene. For a given temperature T, eq 7 can be numerically solved to determine the associated chemical potential $\mu(T)$.

To account for the duration of the pump pulse in our experiment, which is of the same order of magnitude as the carrier relaxation time, the temporal evolution of the carrier temperature is calculated by numerically solving eq 2 via the Euler's method, assuming a 5.5 ps Gaussian input pulse $I(t)$. At each time-step, the chemical potential, Drude weight, plasmon frequency, conductivity, and fractional absorption for the subsequent time step were adjusted based upon eqs 7, 4, 5, 1, and 3, respectively. The step size for this calculation is an order of magnitude smaller than the duration of the pump pulse to minimize the error caused by this step-by-step solution. Knowing the instantaneous temperature transient $T(t)$, the fractional change in probe transmission is then numerically computed as a function of the pump−probe delay Δt using a correlation integral.

The results from the thermal model (Figure 3b) are in close agreement with the experimental data (Figure 3a) and correctly predict the 10 ps response time. This agreement suggests that nonthermal nonlinearities in graphene, which were theoretically proposed in recent studies,[30,31] are weak in our experiment. The increased transmission is a result of a decreased plasmon frequency, which is caused by a reduced value of the chemical potential at elevated electron temperatures (cf. eqs 7 and 4), and a broadening of the resonance caused by a faster scattering rate. While both effects lead to an increased transmission at resonance, the calculations show an decreased transmission for

DOI: 10.1021/acs.nanolett.6b00405
Nano Lett. 2016, 16, 2734−2738

photon frequency below the plasmon resonance (see Section S5). At higher fluence, our measurements show a longer tail that is not reproduced by the model. This slight discrepancy might be caused by a bottleneck in the phonon heating,[32] which was not included in our model. Figure 3c plots the peak value of the (observed and calculated) transient response as a function of the incident pump fluence F, which shows an approximate $F^{1/2}$ dependence. Along the right axis, we plot the corresponding simulated peak electron temperature as a function of fluence, showing the expected $F^{1/3}$ dependence. The observed power scaling was best matched by assuming supercollision cooling as the single dominant cooling mechanism, together with temperature-dependent momentum scattering through LA phonons.[27,29]

Only two free parameters were used in the numerical simulations: the acoustic deformation potential V_D and the electron disorder mean free path l, which together control the strength of dominant cooling and scattering mechanisms. The observed $F^{1/2}$ power scaling seen in Figure 3c was matched by choosing V_D = 11 eV, which is consistent with values reported in the literature for similar graphene.[26,33] The mean free path l was adjusted to match the overall magnitude of the nonlinearity from which we obtained l = 1 nm, which is smaller than that expected from the scattering rate but consistent with other recent experimental measurements of cooling in large-area graphene.[33] The origin of this discrepancy remains to be explained.

To confirm the plasmonic enhancement of the nonlinearity, we repeated the pump–probe measurements with the pump and probe copolarized in the direction parallel to the graphene ribbons, thus ensuring that the plasmons are not excited. Figure 4a compares the measurements from the two polarization cases for the same incident pump fluence and frequency. The measured nonlinearity is far stronger when the plasmons are excited than for the opposite polarization, consistent with the thermal predictions. Figure 4b shows the electric field profile at the plasmon resonance, estimated by frequency-domain finite element calculations, showing the dramatic field enhancement that occurs near the graphene sheet, which contributes to the enhanced nonlinearity.

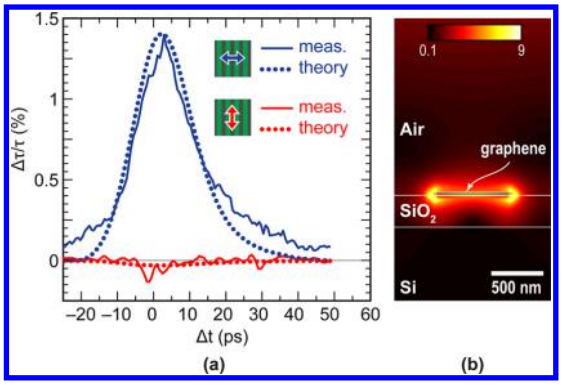

Figure 4. (a) Comparison of normalized change in transmission for two different polarizations. The blue curves show the measured and simulated pump–probe response when the pump and probe were polarized perpendicular to the graphene nanoribbons, thereby exciting the plasmon. The red curves show the measured and simulated response for the same incident pump fluence but opposite polarization, where there is no plasmonic excitation, and the nonlinear response is correspondingly much lower. (b) Electric field profile at the resonant frequency, calculated using a (linear) finite element time domain method with a normally incident wave from above, showing the field-enhancement at the graphene surface. The color indicates the electric field intensity $|\mathbf{E}|^2$, relative to that of the incident plane wave, showing a nearly 9-fold intensity enhancement at the graphene surface.

Figure 5 presents a calculation of how this nonlinearity would be further enhanced by employing higher quality

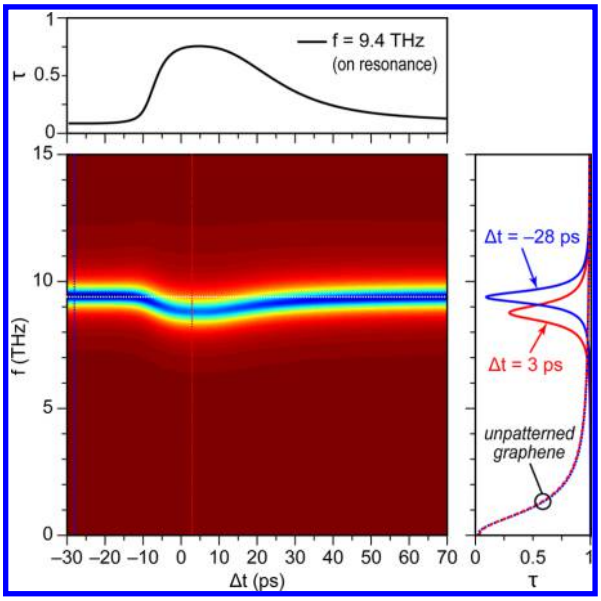

Figure 5. Numerically predicted change in transmission as a function of frequency f and time Δt, calculated assuming a higher graphene mobility of 25 100 cm^2 V^{-1} s^{-1}. The pump pulse causes a transient red shift and broadening of the plasmon resonance, as shown by the two vertical sections plotted on the right. The dashed curves indicated in the right panel show the calculated Drude response for an unpatterned graphene sheet, which shows no plasmon resonance, and very little pump-induced change in transmission. A signal tuned to the resonant frequency would experience a corresponding transient increase in transmission, as shown in the horizontal section plotted on the top.

graphene nanoribbons with a realistic mobility of 25 100 cm^2 V^{-1} s^{-1}.[34] The calculated power transmission is shown as a function of frequency (in the vertical direction) and time (in the horizontal direction), assuming an input fluence of 1.27 μJ/cm^2. The upper horizontal plot shows the calculated pump-induced change in transmission at the equilibrium plasmon resonance frequency (marked by the horizontal white line), showing a nonlinear response in the order of unity. The right vertical plot in Figure 5 shows the calculated transmission spectrum before and during the pump pulse (marked by the vertical white lines), illustrating the nature of plasmonic enhancement in the nonlinearity. The resonant absorption causes a significant increase in the carrier temperature, which leads to (i) a broadening of the plasmon line width caused by an increased carrier scattering (ii) a corresponding weakening of the plasmon resonance and (iii) a red shift of the plasmon resonance. While the first two effects also occur for traditional Drude absorption in graphene, albeit at lower frequencies, the third is unique to plasmon resonances and only occurs in patterned graphene structures. For the experimental conditions considered here, all three effects contribute similarly to the observed response. For high quality graphene, as shown in the right panel of Figure 5, red shift of plasmon frequency has the most substantial impact on transmission.

DOI: 10.1021/acs.nanolett.6b00405
Nano Lett. 2016, 16, 2734–2738

To conclude, the temperature dependent absorption, cooling, and scattering of hot electrons in graphene causes a nonlinear response to terahertz waves. Using terahertz pump−probe measurements, we show that when graphene is patterned into subwavelength structures that exhibit a plasmon resonance, this nonlinearity is greatly enhanced at the resonant frequency. This enhanced nonlinearity is caused by a stronger on-resonance absorption, followed by a spectral red shift and broadening of the plasmon resonance with electron temperature. We provide a thermal model that explains the observed nonlinear enhancement and sheds light on the dominant cooling and scattering mechanisms for hot electrons collectively excited in a graphene plasmon. The theory predicts that in higher-mobility graphene the nonlinearity in transmission could approach unity, enabling high-speed terahertz-induced switching or modulation.

■ ASSOCIATED CONTENT

Supporting Information

The Supporting Information is available free of charge on the ACS Publications website at DOI: 10.1021/acs.nanolett.6b00405.

The Supporting Information contains five subsections: details about (1) the equivalent circuit model, (2) the calculation of the optical parameters of graphene via the Drude model, (3) and the Drude Lorentz model, and discussion about the fluence (4) and frequency (5) dependence of the pump−probe signals. (PDF)

■ AUTHOR INFORMATION

Corresponding Author

*E-mail: mmjadidi@umd.edu.

Notes

The authors declare no competing financial interest.

■ ACKNOWLEDGMENTS

This work was sponsored by the U.S. ONR (N000141310865) and the U.S. NSF (ECCS 1309750). Support from P. Michel and the FELBE-team is gratefully acknowledged. The sample fabrication was carried out at the University of Maryland Nanocenter. We thank Nolan Ballew for technical assistance.

■ REFERENCES

(1) Mikhailov, S.; Ziegler, K. *J. Phys.: Condens. Matter* **2008**, *20*, 384204.
(2) Hendry, E.; Hale, P. J.; Moger, J.; Savchenko, A. K.; Mikhailov, S. A. *Phys. Rev. Lett.* **2010**, *105*, 097401.
(3) Zhang, H.; Tang, D. Y.; Zhao, L. M.; Bao, Q. L.; Loh, K. P. *Opt. Express* **2009**, *17*, 17630−17635.
(4) Hong, S.-Y.; Dadap, J. I.; Petrone, N.; Yeh, P.-C.; Hone, J.; Osgood, R. M. *Phys. Rev. X* **2013**, *3*, 021014.
(5) Zhang, H.; Virally, S.; Bao, Q.; Ping, L. K.; Massar, S.; Godbout, N.; Kockaert, P. *Opt. Lett.* **2012**, *37*, 1856−1858.
(6) Jnawali, G.; Rao, Y.; Yan, H.; Heinz, T. F. *Nano Lett.* **2013**, *13*, 524−530.
(7) Shi, S.-F.; Tang, T.-T.; Zeng, B.; Ju, L.; Zhou, Q.; Zettl, A.; Wang, F. *Nano Lett.* **2014**, *14*, 1578−1582.
(8) Hwang, H. Y.; Brandt, N. C.; Farhat, H.; Hsu, A. L.; Kong, J.; Nelson, K. A. *J. Phys. Chem. B* **2013**, *117*, 15819−15824.
(9) Kadi, F.; Winzer, T.; Malic, E.; Knorr, A.; Göttfert, F.; Mittendorff, M.; Winnerl, S.; Helm, M. *Phys. Rev. Lett.* **2014**, *113*, 035502.
(10) Mics, Z.; Tielrooij, K.-J.; Parvez, K.; Jensen, S. A.; Ivanov, I.; Feng, X.; Müllen, K.; Bonn, M.; Turchinovich, D. *Nat. Commun.* **2015**, *6*, 7655.
(11) Koppens, F. H. L.; Chang, D. E.; García de Abajo, F. J. *Nano Lett.* **2011**, *11*, 3370−3377.
(12) Kauranen, M.; Zayats, A. V. *Nat. Photonics* **2012**, *6*, 737−748.
(13) Ju, L.; Geng, B.; Horng, J.; Girit, C.; Martin, M.; Hao, Z.; Bechtel, H. A.; Liang, X.; Zettl, A.; Shen, Y. R.; Wang, F. *Nat. Nanotechnol.* **2011**, *6*, 630−634.
(14) Brar, V. W.; Jang, M. S.; Sherrott, M.; Lopez, J. J.; Atwater, H. A. *Nano Lett.* **2013**, *13*, 2541−2547.
(15) Yan, H.; Low, T.; Zhu, W.; Wu, Y.; Freitag, M.; Li, X.; Guinea, F.; Avouris, P.; Xia, F. *Nat. Photonics* **2013**, *7*, 394−399.
(16) Jadidi, M. M.; Sushkov, A. B.; Myers-Ward, R. L.; Boyd, A. K.; Daniels, K. M.; Gaskill, D. K.; Fuhrer, M. S.; Drew, H. D.; Murphy, T. E. *Nano Lett.* **2015**, *15*, 7099−7104.
(17) Manjavacas, A.; Nordlander, P.; García de Abajo, F. J. *ACS Nano* **2012**, *6*, 1724−1731.
(18) Gullans, M.; Chang, D. E.; Koppens, F. H. L.; de Abajo, F. J. G.; Lukin, M. D. *Phys. Rev. Lett.* **2013**, *111*, 247401.
(19) Yao, X.; Tokman, M.; Belyanin, A. *Phys. Rev. Lett.* **2014**, *112*, 055501.
(20) Jablan, M.; Chang, D. E. *Phys. Rev. Lett.* **2015**, *114*, 236801.
(21) Chen, P.-Y.; Alù, A. *IEEE Trans. Terahertz Sci. Technol.* **2013**, *3*, 748−756.
(22) Cai, X.; Sushkov, A. B.; Jadidi, M. M.; Nyakiti, L. O.; Myers-Ward, R. L.; Gaskill, D. K.; Murphy, T. E.; Fuhrer, M. S.; Drew, H. D. *Nano Lett.* **2015**, *15*, 4295−4302.
(23) Winnerl, S.; Orlita, M.; Plochocka, P.; Kossacki, P.; Potemski, M.; Winzer, T.; Malic, E.; Knorr, A.; Sprinkle, M.; Berger, C.; de Heer, W. A.; Schneider, H.; Helm, M. *Phys. Rev. Lett.* **2011**, *107*, 237401.
(24) Song, J. C. W.; Reizer, M. Y.; Levitov, L. S. *Phys. Rev. Lett.* **2012**, *109*, 106602.
(25) Viljas, J. K.; Heikkilä, T. T. *Phys. Rev. B: Condens. Matter Mater. Phys.* **2010**, *81*, 245404.
(26) Kar, S.; Mohapatra, D. R.; Freysz, E.; Sood, A. K. *Phys. Rev. B: Condens. Matter Mater. Phys.* **2014**, *90*, 165420.
(27) Das Sarma, S.; Adam, S.; Hwang, E. H.; Rossi, E. *Rev. Mod. Phys.* **2011**, *83*, 407−470.
(28) Frenzel, A. J.; Lui, C. H.; Shin, Y. C.; Kong, J.; Gedik, N. *Phys. Rev. Lett.* **2014**, *113*, 056602.
(29) Chen, J.-H.; Jang, C.; Xiao, S.; Ishigami, M.; Fuhrer, M. S. *Nat. Nanotechnol.* **2008**, *3*, 206−209.
(30) Cox, J. D.; García de Abajo, F. J. *Nat. Commun.* **2014**, *5*, 5725.
(31) Manzoni, M. T.; Silveiro, I.; García de Abajo, F. J.; Chang, D. E. *New J. Phys.* **2015**, *17*, 083031.
(32) Wang, H.; Strait, J. H.; George, P. A.; Shivaraman, S.; Shields, V. B.; Chandrashekhar, M.; Hwang, J.; Rana, F.; Spencer, M. G.; Ruiz-Vargas, C. S.; Park, S. *Appl. Phys. Lett.* **2010**, *96*, 081917.
(33) McKitterick, C. B.; Rooks, M. J.; Prober, D. E. *Phys. Rev. B: Condens. Matter Mater. Phys.* **2016**, *93*, 075410.
(34) Wang, L.; Meric, I.; Huang, P. Y.; Gao, Q.; Gao, Y.; Tran, H.; Taniguchi, T.; Watanabe, K.; Campos, L. M.; Muller, D. A.; Guo, J.; Kim, P.; Hone, J.; Shepard, K. L.; Dean, C. R. *Science* **2013**, *342*, 614−617.

DOI: 10.1021/acs.nanolett.6b00405
Nano Lett. 2016, 16, 2734−2738